JCTC Journal of Chemical Theory and Computation

Article

pubs.acs.org/JCTC

# Quantum-Chemical Studies on Excitation Energy Transfer Processes in BODIPY-Based Donor–Acceptor Systems

J. Dominik Spiegel,[†] Martin Kleinschmidt,[†] Alexander Larbig,[†] Jörg Tatchen,[‡] and Christel M. Marian*[,†]

[†]Institute of Theoretical and Computational Chemistry, Heinrich Heine University Düsseldorf, Universitätsstr. 1, D-40225 Düsseldorf, Germany

[‡]Departamento de Química, Universidad de los Andes, Car. 1 No. 18A-12, Bogotá, Colombia

**ABSTRACT:** BODIPY-based excitation energy transfer (EET) cassettes are experimentally extensively studied and serve as excellent model systems for the investigation of photophysical processes, since they occur in any photosynthetic system and in organic photovoltaics. In the present work, the EET rates in five BODIPY-based EET cassettes in which anthracene serves as the donor have been determined, employing the monomer transition density approach (MTD) and the ideal dipole approximation (IDA). To this end, a new computer program has been devised that calculates the direct and exchange contributions to the excitonic coupling (EC) matrix element from transition density matrices generated by a combined density functional and multireference configuration interaction (DFT/MRCI) calculation for the monomers. EET rates have been calculated according to Fermi's Golden Rule from the EC and the spectral overlap, which was obtained from the calculated vibrationally resolved emission and absorption spectra of donor and acceptor, respectively. We find that the direct contribution to the EC matrix element is dominant in the studied EET cassettes. Furthermore, we show that the contribution of the molecular linker to the EET rate cannot be neglected. In our best fragment model, the molecular linker is attached to the donor moiety. For cassettes in which the transition dipole moments of donor and acceptor are oriented in parallel manner, our results confirm the experimental findings reported by Kim et al. [*J. Phys. Chem. A* **2006**, *110*, 20−27]. In cassettes with a perpendicular orientation of the donor and acceptor transition dipole moments, dynamic effects turn out to be important.

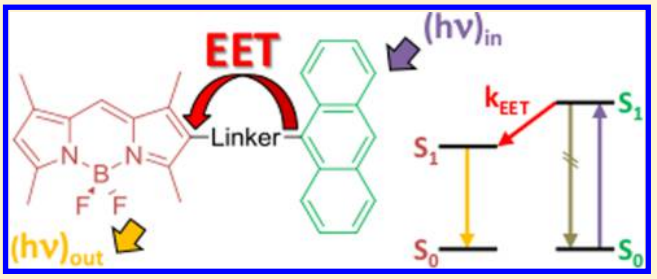


## 1. INTRODUCTION

Excitation energy transfer (EET) is one of the key issues in organic photovoltaics. In a system in which donor and acceptor molecules are covalently linked, EET can take place in two different ways. The limiting case of through-space excitation energy transfer (TSEET) is based on the interaction between a de-excitation process on the donor and a simultaneous excitation process on the acceptor. In 1948, Förster coined the term "direct coupling" for the coupling between a locally excited donor interacting with an acceptor through a Coulomb potential.[1] In 1953, Dexter showed that there is also an exchange contribution to the excitonic coupling (EC), which becomes more and more important as the donor−acceptor distance gets smaller.[2] Dexter explained this type of EET as a simultaneous exchange of electrons between donor and acceptor. In the limiting case of through-bond excitation energy transfer (TBEET), the excitation energy is directly transferred through the molecular bridge linking the donor and the acceptor. The superexchange mechanism proposed by McConnell in 1961[3,4] describes the EET as a tunneling process where the EET rate decreases exponentially with the length of the linker. In a realistic EET system in which donor and acceptor are joined in a single molecule, both TSEET and TBEET coexist and contribute to the EET rate.

### 1.1. The Excitonic Coupling Matrix Element.

The EC matrix element $V_{DA}$ between an excitation on molecule A and a de-excitation on molecule D can be derived, considering the Hamiltonian of a bimolecular system AD.[5] The Hamiltonian is given by the sum of the electronic Hamiltonian, the operator of the kinetic energy of the nuclei, and the operator of the internuclear repulsion:

$$\hat{H}(R) = \hat{H}_{el}(R) + \hat{T}_{nuc}(R) + \hat{V}_{(nuc-nuc)}(R) \quad (1)$$

Herein, $R$ is the set of coordinates of all nuclei. Assuming that the total system can be decomposed into two individual molecules A and D, intramolecular and intermolecular coordinates can be separated. In this case, the electronic Hamiltonian of the bimolecular system can be written as the sum of the electronic Hamiltonians of A and D and the interaction $\hat{V}_{DA}^{(el-el)}$ between the electrons located at the two molecules consisting of a direct and an exchange term.

$$\hat{H}_{el}(R) = \hat{H}_{D}^{(el)}(R) + \hat{H}_{A}^{(el)}(R) + \frac{1}{2}\hat{V}_{DA}^{(el-el)}(R) \quad (2)$$

The potential $\hat{V}_{DA}^{(el-el)}$ is responsible for the EC. The electronic wave function of the total system $\phi_{a,d}$ is expanded

**Received:** May 27, 2015
**Published:** July 27, 2015





DOI: 10.1021/acs.jctc.5b00501
*J. Chem. Theory Comput.* 2015, 11, 4316−4327

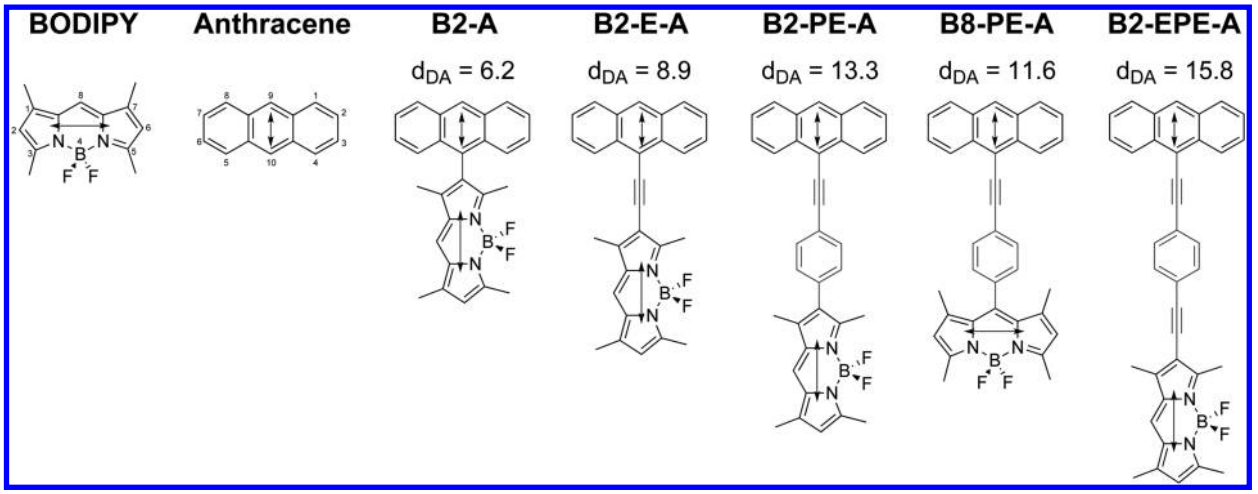


**Figure 1.** Nomenclature and chemical structure of studied EET cassettes. The $S_0 \rightarrow S_1$ transition dipole moments of BODIPY and anthracene are indicated as arrows. Distances between the centers of mass are given in Ångstroms.

as antisymmetrized product of the adiabatic electronic states of the individual systems

$$\phi_{a,d}(r_m, R) = \hat{\mathcal{A}}[\varphi_{Aa}(r_A, R)\varphi_{Dd}(r_d, R)] \tag{3}$$

where $r_A$ and $r_D$ denote the electronic coordinates of A and D, respectively, and "a" and "d" label the respective local electronic states. $\hat{\mathcal{A}}$ represents the antisymmetrization operator:

$$\hat{\mathcal{A}} = \frac{1}{\sqrt{N_p}} \sum_{\text{perm}} (-1)^p \hat{P} \tag{4}$$

where $\hat{P}$ generates permutations of the electron coordinates of molecules A and D in the total system and $p$ is the number of transpositions. The total number of permutations $N_p$ is dependent on the number of electrons of the individual systems and is given by

$$N_p = \frac{(N_{el}^{(A)} + N_{el}^{(D)})!}{(N_{el}^{(A)}! N_{el}^{(D)}!)!} \tag{5}$$

Note that the resulting states of the total system are not orthonormal.

The EC matrix element between a local transition on molecule A from state $a_1$ to $a_2$ and a local transition on molecule D from state $d_1$ to $d_2$ is then given by

$$\begin{aligned}\langle \phi_{a_2 d_2} | \hat{V}_{DA}^{(el-el)} | \phi_{a_1 d_1} \rangle &= \int dr_A\, dr_D\, (\hat{\mathcal{A}}[\varphi_{a_2}(r_A, R)\varphi_{d_2}(r_D, R)]) \cdot \hat{V}_{DA}^{(el-el)} \\ &\quad \cdot (\hat{\mathcal{A}}[\varphi_{a_1}(r_A, R)\varphi_{d_1}(r_D, R)]) \\ &\equiv J_{DA} + K_{DA}\end{aligned} \tag{6}$$

where $J_{DA}$ is the direct contribution and $K_{DA}$ is the exchange contribution. $K_{DA}$ is dependent on the spatial overlap of molecular orbitals located at A and those located at D.

If the exchange contribution $K_{DA}$ is neglected, the electronic state of the total system can be written as a Hartree product of the local electronic states:

$$\phi_{a,d}^{HP}(r_A, r_D, R) = \varphi_a(r_A, R)\varphi_d(r_D, R) \tag{7}$$

such that the right-hand side of eq 6 simplifies to the direct contribution term:

$$\langle \phi_{a_2 d_2} | \hat{V}_{DA}^{(el-el)} | \phi_{a_1 d_1} \rangle \approx \langle \varphi_{a_2} \varphi_{d_2} | \hat{V}_{DA}^{(el-el)} | \varphi_{a_1} \varphi_{d_1} \rangle = J_{DA} \tag{8}$$

**1.2. The Energy Transfer Rate.** The EET process is termed incoherent if it takes place on a much longer time scale than intermolecular and intramolecular relaxation ($\tau_{trans} \gg \tau_{relax}$). In this case, the EET rate can be described by a Golden Rule expression, which has already been applied successfully to such processes in the past.[6−8]

$$\begin{aligned}k_{EET} = \frac{2\pi}{\hbar} \sum_{MN} \sum_{KL} f(E_{D^*M}) f(E_{AL}) |\langle \Psi_{DN} \Psi_{A^*K} | \hat{V}_{DA}^{(el-el)} | \Psi_{D^*M} \Psi_{AL} \rangle|^2 \\ \times \delta(E_{D^*M} + E_{AL} - E_{DN} - E_{A^*K})\end{aligned} \tag{9}$$

where $f(E_{D^*M})$ is the thermal occupation of the vibrational state M of the electronically excited donor molecule with vibronic wave function $\Psi_{D^*M}$ and energy $E_{D^*M}$. Similarly, $f(E_{AL})$ denotes the thermal occupation of the vibrational state $L$ of the acceptor molecule in the electronic ground state with vibronic wave function $\Psi_{AL}$ and energy $E_{AL}$, etc. The delta distribution term ($\delta$) ensures that only energy-conserving processes contribute to the EET rate. Assuming that the electronic part of the EC is not dependent on the nuclear coordinates (Condon approximation), the coupling matrix element becomes

$$\langle \Psi_{A^*K} \Psi_{DN} | \hat{V}_{DA}^{(el-el)} | \Psi_{D^*M} \Psi_{AL} \rangle = V_{DA} \langle \chi_{AL} | \chi_{A^*K} \rangle \langle \chi_{D^*M} | \chi_{DN} \rangle \tag{10}$$

where the $\chi$ denote purely vibrational wave functions of the donor and acceptor molecules in the electronic ground and excited states, respectively. The EET rate then reads as follows:

$$\begin{aligned}k_{EET} = \frac{2\pi}{\hbar} |V_{DA}|^2 \sum_{MN} \sum_{KL} f(E_{AL}) f(E_{D^*M}) |\langle \chi_{AL} | \chi_{A^*K} \rangle|^2 \langle \chi_{D^*M} | \chi_{DN} \rangle \\ \times \delta(E_{D^*M} + E_{AL} - E_{A^*K} - E_{DN})\end{aligned} \tag{11}$$

The Franck−Condon weighted density of states (FCWD)[9,10] is typically approximated as the spectral overlap of the normalized donor emission $F_D(\omega)$ and the acceptor absorption spectrum $A_A(\omega)$. In this case, the EET rate is given by[5,6]

$$k_{EET} = \frac{2\pi}{\hbar} |V_{DA}|^2 \int_0^\infty F_D(\omega) A_A(\omega)\, d\omega \tag{12}$$

**1.3. Energy Transfer Cassettes.** Because of their physical and chemical properties, donor−acceptor systems based on 4,4-difluoro-4-bora-3a,4a-diaza-*s*-indacene (BODIPY) are eligible



DOI: 10.1021/acs.jctc.5b00501
J. Chem. Theory Comput. 2015, 11, 4316−4327

candidates for use in organic photovoltaics.[11−15] BODIPY dyes are characterized by strong absorption of UV light and sharp fluorescence with high quantum yields.[16] The compounds are largely insensitive to the pH and polarity of the solvent. BODIPY itself is reported to be chemically unstable and therefore has not been synthesized until now.[16] Within this article, we use BODIPY as an abbreviation for the 1,3,5,7-methylated derivate. Alkylated compounds barely differ in their absorption and emission spectra. Vertical absorption and emission energies of BODIPY have been calculated by Briggs et al. at the CAS-PT2 and Restricted Open-Shell Kohn−Sham levels, respectively.[17]

Cassettes in which BODIPY is covalently linked to a second chromophore are experimentally and extensively studied and serve as model systems for the description of EET processes. In this work, we present theoretical studies on the EET in five different BODIPY-based cassettes (see Figure 1). In all investigated systems, BODIPY serves as the acceptor while anthracene serves as the donor. Experimentally obtained fluorescence lifetimes and EET rates of these cassettes were reported by Kim and Wan.[18,19] To the best of our knowledge, no theoretical studies of EET processes in the investigated BODIPY-based EET cassettes have been conducted so far. A theoretical study of the EET in another BODIPY-based dyad mainly concentrating on solvent screening effects was reported by Caprasecca et al.[20]

In this work, we use a monomer-based approach to calculate the EC and determine the EET rate. The obtained results are compared to experimental data and confirm the assumption that the through-space contribution to the EC is dominant.

## 2. THEORETICAL METHODS

In practice, there are two main approaches to calculate the EC matrix element.[21] In calculations that are based on a supermolecular description of the entire system, the full EC can directly be deduced from the energetic splitting of the involved excited states. In the case of unsymmetric systems, the eigenstates of the Hamiltonian must be transformed to a diabatic basis first.[22,23] In monomer-based approaches, the individual contributions to the EC must be computed from physical quantities obtained from separate quantum-chemical calculations of the donor and acceptor parts of the total system. Within this paper, we employ the monomer transition density (MTD) approach,[24−26] the ideal dipole approximation (IDA)[1,27] as well as the symmetric energy splitting method (Davydov Splitting),[28,29] which are outlined in the following. A detailed derivation of the EC has been given by May and Kühn.[5]

**2.1. Exact Excitonic Coupling.** The exact EC of homodimers, including direct and exchange contributions, can be calculated from the symmetric energetic splitting of the appropriate monomer excited states in a supermolecular calculation.

$$V_{AA} = \frac{E_2 - E_1}{2} \tag{13}$$

Since the method is not applicable to heterodimeric systems, approximate approaches based on monomer calculations are applied.

**2.2. Monomer Transition Density Approach.** Starting from eq 8, the EC matrix element can be regarded as an interaction between two transition densities located on monomers D and A.[24,25] Within the MO basis, a transition density is expressed in the form of a matrix. The spinless reduced one-particle transition density matrix connecting the electronic states $\Psi_{a_1}$ and $\Psi_{a_2}$ of an $N$-electron system A is defined as[30]

$$\rho(a_1 a_2 | r_1;\, r_1') = N \int\int \cdots \int \Psi^*_{a_2}(x'_1,\, x_2, ..., x_N) \times \Psi_{a_1}(x_1,\, x_2, ..., x_N)\, \mathrm{d}s_1\, \mathrm{d}x_2 \ldots \mathrm{d}x_N \tag{14}$$

A similar expression is obtained for subsystem D. Let $i$ and $j$ be molecular orbitals (MOs) located on monomer A and $k$ and $l$ are MOs located on monomer D. Evaluating the transition density matrices in the MO basis yields

$$J_{DA} = \sum_{ijkl} \rho_{ij}^{(A)} (ij|kl) \rho_{kl}^{(D)} \tag{15}$$

where we have used the Mulliken convention for denoting the electronic repulsion integral. Following Fujimoto,[26] the exchange contribution to the EC can be approximated in analogy to the direct contribution by

$$K_{DA} = -\frac{1}{2} \sum_{ijkl} \rho_{ij}^{(A)} (il|kj) \rho_{kl}^{(D)} \tag{16}$$

The total coupling is the sum of direct and exchange contributions.

$$V_{DA} = J_{DA} + K_{DA} \tag{17}$$

**2.3. Ideal Dipole Approximation.** If the intermolecular distance $X_{DA}$ is large compared to the intramolecular extensions of molecules A and D, the intermolecular Coulomb interaction can be subjected to a multipole expansion, which is truncated after the dipole−dipole contribution.

$$V_{DA} = \sum_{jk} \frac{e^2}{|\vec{X}_{DA} + \vec{r}_j^{(A)} - \vec{r}_k^{(D)}|} = \sum_{jk} \frac{e^2}{|\vec{X}_{DA} + \vec{r}_{jk}|} \tag{18}$$

$$\approx e^2 \sum_{jk} \frac{1}{|\vec{X}_{DA}|} + \vec{r}_{jk} \cdot \vec{\nabla} \frac{1}{|\vec{X}_{DA}|} - \frac{1}{2} (\vec{r}_{jk} \vec{r}_{jk} \cdot \vec{\nabla})(\vec{r}_{jk} \cdot \vec{\nabla}) \frac{1}{|\vec{X}_{DA}|} \tag{19}$$

$$\approx e^2 \sum_{jk} \frac{1}{|\vec{X}_{DA}|} - \frac{\vec{r}_{jk} \cdot \vec{X}_{DA}}{|\vec{X}_{DA}|^3} - \frac{1}{2} \left( \frac{\vec{r}_{jk}^{\,2}}{|\vec{X}_{DA}|^3} - 3 \frac{(\vec{r}_{jk} \cdot \vec{X}_{DA})^2}{|\vec{X}_{DA}|^5} \right) \tag{20}$$

Herein, $j$ denotes the $j$th electron of molecule A and $k$ is the $k$th electron of molecule D. The first- and second-order terms, as well as parts of the third-order term, vanish because of the charge neutrality of the individual molecules. Employing the definition of the transition dipole moments,

$$\vec{\mu}_A = e \sum_j \vec{r}_j^{(A)} \quad \text{and} \quad \vec{\mu}_D = e \sum_k \vec{r}_k^{(D)} \tag{21}$$

of molecules A and D, respectively, the term finally reads

$$V_{DA} = \frac{\vec{\mu}_A \vec{\mu}_D}{|\vec{X}_{DA}|^3} - 3 \left[ \frac{(\vec{\mu}_A \vec{X}_{DA})(\vec{\mu}_D \vec{X}_{DA})}{|\vec{X}_{DA}|^5} \right] \tag{22}$$

Introducing unit vectors pointing in the directions of the intermolecular distance vector $\vec{e}_{DA}$, which is defined as


DOI: 10.1021/acs.jctc.5b00501
J. Chem. Theory Comput. 2015, 11, 4316−4327

$$\vec{e}_{DA} = \frac{\vec{X}_{DA}}{|\vec{X}_{DA}|}$$

and the directions of the transition dipole moments $\vec{n}_D$ and $\vec{n}_A$, which are defined, respectively, as

$$\vec{n}_D = \frac{\vec{\mu}_D}{|\vec{\mu}_D|}$$

and

$$\vec{n}_A = \frac{\vec{\mu}_A}{|\vec{\mu}_A|}$$

the EC matrix element can be expressed in the familiar form

$$V_{DA} = \kappa_{DA} \frac{|\vec{\mu}_A| \cdot |\vec{\mu}_D|}{|\vec{X}_{DA}|^3} \quad (23)$$

where $\kappa_{DA}$ is the so-called orientation factor,

$$\kappa_{DA} = \vec{n}_A \vec{n}_D - 3(\vec{e}_{DA}\vec{n}_A)(\vec{e}_{DA}\vec{n}_D) \quad (24)$$

**2.4. Computational Details.** The equilibrium geometries of the singlet ground states ($S_0$) of the EET cassettes and the individual monomers were optimized using density functional theory (DFT), in conjunction with the B3LYP hybrid functional.[31] The molecular structures of the first excited singlet states ($S_1$) of both BODIPY and anthracene were optimized using time-dependent density functional theory (TDDFT). Unless otherwise stated, all calculations were performed with TURBOMOLE 6.5,[32] employing a basis set of split valence quality with polarization functions on all atoms (SVP).[33] For the optimization of the minimum geometries of the EET cassettes and coordinate scans, the m5 integration grid was used. Frequency analyses at the $S_0$ and $S_1$ minimum geometries were carried out using the SNF program package.[34] Unrelaxed torsion angle scans of the EET cassettes were performed along selected internal coordinates starting from preoptimized $C_s$-symmetric structures in which the planes of BODIPY and anthracene are perpendicularly oriented.

The photophysical properties at the ground- and excited-state minima of the monomers (vertical transition energies, transition density matrices, and transition dipole moments) were calculated using the combined density functional and multireference configuration interaction (DFT/MRCI) program.[35] In these calculations, Kohn–Sham orbitals of a ground-state calculation employing the BHLYP functional[36] were utilized. The two-electron integrals used in the DFT/MRCI and MTD calculations were approximated with the resolution of the identity method, as given by

$$(ij|kl) \approx \sum_{P,Q} (ij|P) \cdot (P|Q)^{-1} \cdot (Q|kl) \quad (25)$$

where $P$ and $Q$ are auxiliary basis sets.[37,38]

In the DFT/MRCI method, dynamic correlation effects are considered by DFT, whereas static correlation effects are taken into account by a MRCI expansion. The configurations used in the MRCI are based on Kohn–Sham orbitals of a closed-shell electronic state. Double-counting of dynamic correlation is avoided by the use of an effective Hamiltonian comprising five empirical parameters that are independent from the target molecule. At present, parameter sets are only available for the BHLYP functional. The MRCI expansion is truncated by considering only orbitals below a certain energy cutoff. Within this paper, we used the original set of parameters[35] and an orbital selection energy threshold of 1.0 $E_H$ to compute the 10 lowest eigenvectors. The initial MRCI reference space was spanned by all single and double excitations from the four highest occupied MOs to the four lowest unoccupied MOs of the ground-state Kohn–Sham determinant. A second DFT/MRCI step was performed with a refined reference space comprising all configurations, which contribute to one of the 10 lowest-lying eigenvectors of the initial DFT/MRCI calculation with a squared coefficient of 0.003 and larger.

To calculate the EET between the donor and the acceptor in the EET cassettes, two fragmentation models were developed, which are based on the work of Caprasecca et al.[39] (Figure 2).

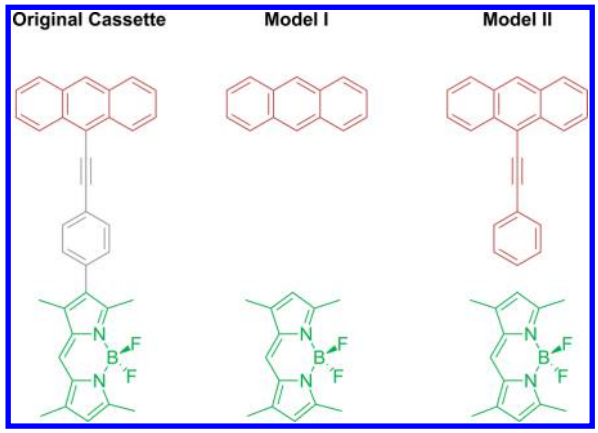


**Figure 2.** Fragmentation models developed to calculate the EC in the studied EET cassettes, using the example of **B2-PE-A**. According to fragmentation model I, the linker is completely removed from the relaxed ground-state structure. Fragmentation model II tries to approximate the influence of the molecular structure of the linker on the EC by assigning the latter to the donor moiety. In both models, the obtained fragments are saturated with hydrogen atoms and the newly created C–H bond were relaxed, keeping the rest of the molecule fixed.

According to fragmentation model I, only the distance between the donor and the acceptor was considered (TSEET). The molecular linker was removed from the optimized ground-state structure and the obtained monomers were saturated with hydrogen atoms. The newly created C–H bonds were relaxed keeping the rest of the molecules fixed. Fragmentation model II aims to take the influence of the molecular linker on the EC into account and, therefore, can also include the through-bond contribution. Based on the analysis of the MOs, the linker was assigned to the donor moiety. The obtained fragments were again saturated with hydrogen and relaxed.

EET rates were calculated from the spectral overlap and EC matrix element according to eq 12. The EC matrix elements were computed according to eqs 13, 17, and 23. To this end, a FORTRAN program (FRECK, which stands for Fragment Excitonic Coupling Kit) was newly devised that is adapted to the DFT/MRCI code. In the framework of IDA, the intermolecular distance $r_{DA}$ serves as a measure for the distance between the coupled transition dipoles. As is common practice, we chose the barycenters of the respective monomers as reference.

Vibrationally resolved absorption and emission spectra of BODIPY and anthracene, respectively, were generated with the VIBES program,[40,41] using a temperature of 298 K, an integration time interval of 3000 fs, and a Gaussian damping


DOI: 10.1021/acs.jctc.5b00501
J. Chem. Theory Comput. 2015, 11, 4316–4327

of the correlation function of a width of 100 $cm^{-1}$. Both spectra were normalized to unit area and the spectral overlap was determined by numerical integration.

To approximate the influence of molecular vibrations on the EC matrix-element-free *ab initio* Born−Oppenheimer molecular dynamic (MD) simulations of all EET cassettes were performed on the ground-state potential energy surfaces (PES) using TURBOMOLE. The program employs the Leapfrog Verlet algorithm[42] to integrate Newton's equation of motion. All simulations were performed in vacuum at a temperature of 298 K. The equilibrium geometries and random initial velocities corresponding to an initial temperature of 298 K were used as starting points for the MD simulations. The integration time step for the MD simulations was set to 1.94 fs. The MD simulations reached a length of 3.87 ps. Conformations saved at 97 fs intervals were used for analysis. The total EET rate was calculated by taking the average of the EET rates of each conformation, neglecting the exchange contribution to the EC and applying fragmentation model I. For **B8-PE-A**, we also used fragmentation model II for comparison.

## 3. RESULTS AND DISCUSSION

**3.1. Benchmark Calculations.** To validate the implementations of the IDA and MTD approaches, benchmark calculations were performed using a $\pi$-stacked ethylene dimer as the model system (Figure 3). For this system, literature data

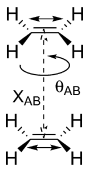


**Figure 3.** Chemical structure of the $\pi$-stacked ethylene dimer used for benchmark calculations. $S_0 \rightarrow S_1$ transition dipole moments are indicated as arrows. The distance $X_{AB}$ between the two $\pi$-stacked monomers is indicated as a dashed arrow. $\theta_{AB}$ denotes the dihedral between the donor and the acceptor.

are availble.[26] EC was calculated for varying intermolecular distances and torsion angles, while the intramolecular geometry parameters were kept fixed to their ground-state values. The exact EC referred to as "FullQM" obtained from half of the Davydov splitting was used as reference.

A DFT/MRCI calculation of an ethylene monomer using the TZVP (SVP) basis set[43] yields a vertical excitation energy of 8.03 eV (154 nm) (8.41 eV (147 nm)) at the ground-state geometry. The experimental absorption spectrum shows a very broad absorption band ranging from 140 nm (8.86 eV) to 172 nm (7.21 eV) with a maximum at ∼161 nm (7.70 eV).[44] Taking into account that the $S_1$ state of ethylene exhibits a strongly displaced minimum geometry with orthogonally twisted $CH_2$ groups[45,46] and considering a fidelity of the DFT/MRCI method of 0.2 eV, the agreement with the experiment is satisfactory. The wave function of the $S_1$ state is composed almost exclusively of the determinant describing the excitation from the highest occupied molecular orbital (HOMO) to the lowest unoccupied molecular orbital (LUMO). A total transition dipole moment of 4.27 D (4.24 D) was found pointing in the direction of the C═C bond.

EC matrix elements at various internuclear distances and orientations are displayed in Figures 4 and 5. When the intermolecular distance of the ethylene $\pi$-stack is increased at a

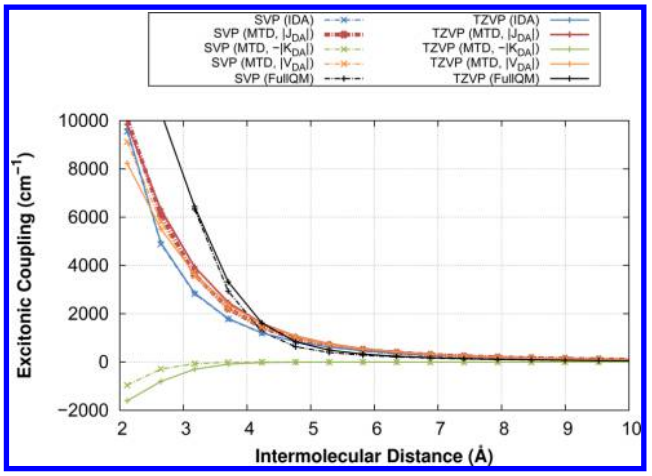


**Figure 4.** Distance and basis set dependency of IDA, MTD, and FullQM calculations on the ethylene $\pi$-stack. $J_{DA}$ denotes the direct contribution to the EC, $K_{DA}$ is the exchange contribution, and $V_{DA}$ is the total through-space EC. "FullQM" denotes the exact EC derived from the Davydov splitting.

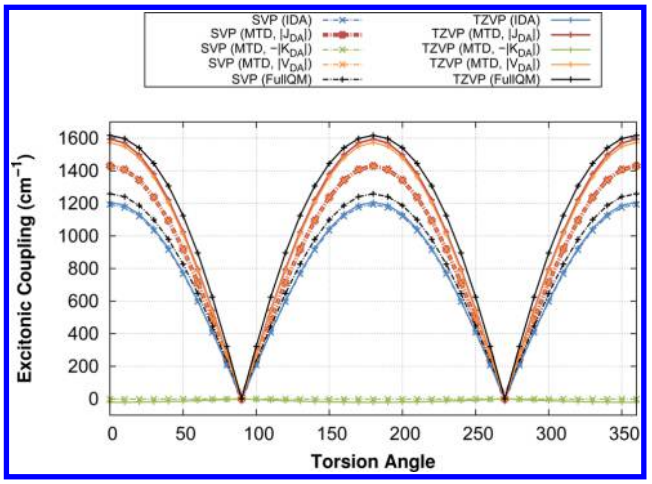


**Figure 5.** Basis set and torsional dependency of IDA, MTD, and FullQM calculations on the ethylene $\pi$-stack for an intermolecular distance of 8 $a_0$ (4.23 Å). (For the denomination of terms, see Figure 4.)

fixed torsion angle of 0°, the direct contribution to the EC decreases as $|\vec{X}_{AB}|^{-3}$ (Figure 4). While the EC obtained from the IDA is almost independent of the basis set, MTD provides slightly higher direct contributions of the EC when the larger TZVP basis set is used. The exchange part of the EC only has an appreciable influence if the intermolecular distance is smaller than ∼4.5 Å. The exchange contribution to the EC is dependent much stronger on the size of the basis set than the direct contribution. This behavior is to be expected, because the exchange interaction is dependent on the orbital overlap between the two molecules. At large intermolecular separations, the approximate methods are seen to perform quite well in comparison with the exact EC obtained from the Davydov splitting. Up to a distance of ∼4.7 Å, the exact EC is somewhat smaller than the MTD and IDA values. When $|\vec{X}_{AB}|$ is decreased further, a crossover of the curves in Figure 4 is observed. Below the typical van der Waals distance, the Davydov splitting rises substantially steeper than $|\vec{X}_{AB}|^{-3}$. This behavior is attributed to the deformation of the $\pi$-orbital densities in the supermolecuar calculation due to Pauli repulsion. In contrast, the shapes of the


DOI: 10.1021/acs.jctc.5b00501
J. Chem. Theory Comput. 2015, 11, 4316−4327

corresponding monomer orbitals employed in the MTD and IDA approximations remain unchanged when the two ethylene molecules come closer.

Varying the torsion angle between the two monomers at a fixed distance of 8 $a_0$ (4.24 Å), the modulus of the EC was found to reach the maximum value when the torsion angle amounts to 0° or 180° where the transition dipole moments are oriented in parallel manner (Figure 3). At the chosen intermolecular distance, the exchange contribution to the total EC is almost negligible. The EC is zero when the MTD moments are pointing in perpendicular directions. This is the case if the torsion angle is 90° or 270°. Between two minima, the EC is described by a reversed parabolically shaped function. These results are in accordance with what has been reported by Fujimoto.[26]

In the SVP basis set, the exact EC obtained from the Davydov splitting has a maximum value of 1259 $cm^{-1}$, while the maximal exact EC amounts to 1617 $cm^{-1}$ when using the larger TZVP basis set. The substantial deviation of 358 $cm^{-1}$ can be traced back to the different representation of the outer parts of the 2$p$ orbitals by the two basis sets. While the most diffuse $p$ Gaussian function exhibits an exponent of 0.1527 in the SVP basis, this spatial region is covered by two freely varying Gaussian functions with exponents of 0.2889 and 0.1005 in the TZVP basis. The EC calculated at the DFT/MRCI level of theory, using the TZVP basis set is in good agreement with the results reported by Fuijmoto for the same system using configuration interaction singles (CIS).

Calculating the EC with the MTD approach, we find only a small deviation from the exact EC when the TZVP basis set is used. If the SVP basis is employed instead, the MTD approximation overestimates the corresponding value derived from the Davydov splitting. These results suggest that the EC in an ethylene dimer can be determined without significant deviation if the MTD approach and at least the TZVP basis set is used.

The EC matrix elements computed using IDA significantly differ from the exact results obtained from the Davydov splitting when the TZVP basis set is used. Employing the smaller SVP basis set, the exact EC matrix elements are described with less accuracy, yielding much smaller results, similar to those obtained from IDA calculations with either the TZVP or SVP basis set. This result confirms the inferior performance of IDA at small distances previously reported by Wong et al.,[27] even if the larger TZVP basis set is used.

Summarizing, we find that the exact EC in a $\pi$-stacked ethylene dimer is strongly dependent on the size of the basis set. MTD is a good approximation as long as at least a basis set of TZVP quality is used. The exchange contribution to the EC coupling matrix element is negligible for intermolecular distances larger than 4.5 Å. The IDA description the EC is not enhanced by the use of the larger TZVP basis instead of the SVP basis. The deviation between the monomer-based calculations and the exact is EC is caused by the fact that the distortion of the electron density of one monomer by the other is not taken into account. Since donor and acceptor are well separated in the studied EET cassettes, the error is considered to be small. In principle, the influence of the electron density of the other monomer could, for example, be considered in a subsystem formalism.[47]

**3.2. Energy Transfer Cassettes.** An overview over the calculated vertical absorption and emission energies of anthracene and BODIPY and corresponding experimental results is given in Table 1.

**Table 1. Calculated Vertical Absorption and Emission Energies, as Well as Corresponding Transition Dipole Moments (TDM) of BODIPY, Anthracene, and the Fragments Used in Fragmentation Model II[a]**

| molecule/ fragment | $\Delta E_{S_0 \rightarrow S_1}$ (eV) [exp] | TDM (D) | $\Delta E_{S_0 \leftarrow S_1}$ (eV) [exp] | TDM (D) |
|---|---|---|---|---|
| BODIPY | 2.64 [2.46][16,54] | 8.0 | 2.53 [2.40][16,54] | 3.2 |
| anthracene | 3.53 [3.60][49−52] | 3.1 | 3.13 [3.12][52,53] | 3.2 |
| **E-A** | 3.22 | 4.3 | | |
| **PE-A** | 2.96 | 6.8 | | |
| **EPE-A** | 2.83 | 8.2 | | |

[a]The energies of the monomers (BODIPY and anthracene) are calculated with respect to their relaxed ground-state geometries. The excitation energies of the fragments are calculated with respect to the relaxed ground-state geometries of the preliminary cassettes after saturation with hydrogen and letting the newly created C−H bond relax.

*3.2.1. Anthracene.* In 2008, some of us already reported on the absorption spectrum of anthracene calculated at the DFT/MRCI level of theory.[48] The relevant results of that study will be reviewed here. We also comment on the calculation of the vibrationally resolved emission spectrum.

The ground and first excited states of anthracene can be classified according to the $D_{2h}$ molecular point group. While the first excited singlet state belongs to the $B_{2u}$ irreducible representation, the electronic ground state has $A_g$ symmetry. The $1^1B_{2u}$ wave function is mainly composed of the HOMO → LUMO excitation and to a minor extent of HOMO−1 → LUMO+1. The involved frontier orbitals are shown in Figure 6. Using the SVP basis set, the vertical excitation energy at the ground-state equilibrium geometry is 3.52 eV (352 nm). When the larger TZVP basis set is employed, the vertical excitation energy does not change significantly. Comparison of these results to the experimental value of 3.60 eV (344 nm)[49−52] suggests that the DFT/MRCI method using a SVP basis describes the $1^1A_g \rightarrow 1^1B_{2u}$ with a sufficient degree of precision. The calculated transition dipole moment has an absolute value of 3.10 D and points in the direction of the short molecular axis (Figure 1).

A DFT/MRCI calculation at the geometry of the optimized $1^1B_{2u}$ state yields a vertical emission energy of 3.13 eV (396 nm, 25 245 $cm^{-1}$). The experimental fluorescence spectrum was measured in cyclohexane and is composed of five peaks at 375 nm (26667 $cm^{-1}$), 397 nm (25189 $cm^{-1}$), 421 nm (23753 $cm^{-1}$), 446 nm (22422 $cm^{-1}$), and 475 nm (21053 $cm^{-1}$).[52,53] The calculated vertical transition with a wavelength of 396 nm corresponds to the experimental peak with the highest intensity at 397 nm. The vibrational frequencies of the $S_0$ and $S_1$ states and the adiabatic excitation energies were used for the calculation of a vibrationally resolved emission spectrum (see Figure 7). The computed emission spectrum has the same shape as the experimental fluorescence spectrum, with a peak at 26 901 $cm^{-1}$ (372 nm) having a shoulder at 26 512 $cm^{-1}$ (377 nm) and a peak at 25 367 $cm^{-1}$ (394 nm) having a shoulder at 24 976 $cm^{-1}$ (400 nm) as well as peaks at 23 861 $cm^{-1}$ (419 nm) and 22 365 $cm^{-1}$ (447 nm).

*3.2.2. BODIPY.* In this work, we used a $C_{2v}$ symmetric BODIPY derivate, which carries four methyl substitutents at



DOI: 10.1021/acs.jctc.5b00501
J. Chem. Theory Comput. 2015, 11, 4316−4327

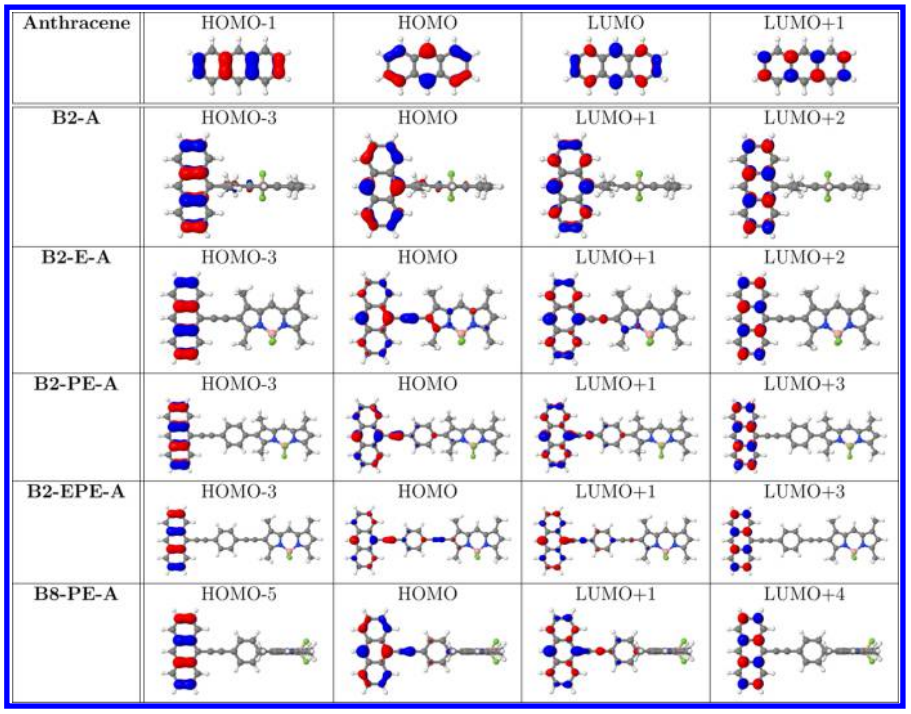


**Figure 6.** Frontier orbitals of anthracene involved in the $S_0 \rightarrow S_1$ transition and their corresponding orbitals computed for the EET cassettes.

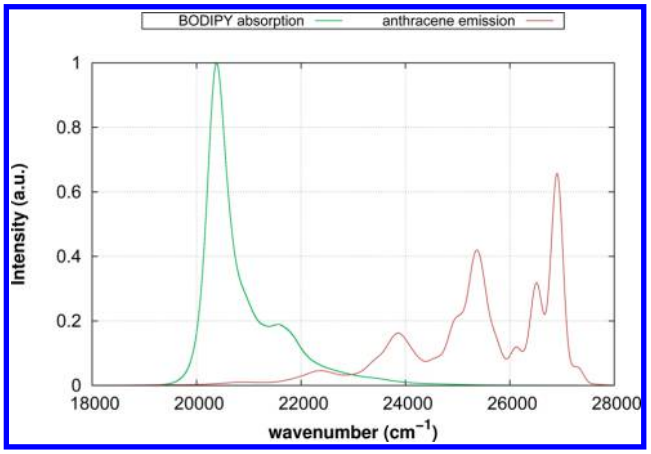


**Figure 7.** Computed vibrationally resolved anthracene emission and BODIPY absorption spectrum.

C1, C3, C5, and C7. Using either the SVP or the TZVP basis set, the first excited singlet state at DFT/MRCI level of theory is the $1^1B_2$ state with a vertical transition energy of 2.63 eV (472 nm). This result agrees well with the experimental absorption maximum of 2.46 eV (505 nm),[16,54] taking into account the precision of the theoretical method used and the fact that the experimental result was measured in ethanol. The $S_1$ state is dominated by the HOMO → LUMO excitation but exhibits also contributions from the HOMO−1 → LUMO excitation and the determinant describing the double excitation HOMO, HOMO−3 → LUMO$^2$. The MOs involved in the $S_0$ → $S_1$ excitation are shown in Figure 8. The vibrationally resolved absorption spectrum (Figure 7) shows a sharp peak of high intensity at ∼20 470 cm$^{-1}$ (489 nm) with a smaller shoulder at 21 571 cm$^{-1}$ (464 nm).

The vertical emission energy, with respect to the optimized $S_1$ state, is 2.52 eV, corresponding to a wavelength of 492 nm, using either the SVP or the TZVP basis sets. This result again agrees well to the experimental emission maximum of 2.40 eV (516 nm) measured in ethanol.[16,54]

### 3.3. Orientation of the Donor and Acceptor Moieties.

To obtain an overview over the potential energy surfaces (PESs) of the EET cassettes, we performed unrelaxed scans along selected internal coordinates (Figure 9). In **B8-PE-A**, the linker was fixed in a perpendicular position, with respect to the BODIPY frame, because of the strong steric repulsion between the phenyl ring of the linker and the methyl groups located at C1 and C7 of the BODIPY moiety, even preventing a coplanar conformation. In **B2-EPE-A** and **B2-PE-A**, the linker was kept in plane with anthracene, since there is no obvious steric interaction between anthracene and the phenyl ring of the linker. The steric repulsion between the methyl groups located at C1 and C3 of the BODIPY moiety and the appropriate phenyl group is much weaker than in **B8-PE-A**. For that reason, the corresponding degree of freedom was scanned in these cases. The torsion angle of the minimum nuclear structure is dependent on the steric repulsion between the donor and the acceptor on the one hand and, as far as possible, the conservation of a planar $\pi$-conjugated system on the other hand. In case of **B2-A**, the donor and the acceptor come very close and torsion angles of 75°−105° can be regarded as a compromise between conservation of the $\pi$-conjugated system and a strong steric repulsion. The methyl groups located at C1 and C3 of BODIPY even prevent a planar conformation. In contrast, in **B2-E-A** and **B2-EPE-A**, an almost planar conformation is preferred because the $\pi$-conjugated system can be conserved on the overall molecule. Assuming structures with an energy lower than $k_BT$ to be thermally occupied, the torsion angle may change up to 35° and 50°, respectively, around the global minimum. In **B2-PE-A** the steric interactions between the methyl groups of BODIPY and the adjacent phenyl ring of the linker determine the torsion angle. We find a global minimum at a torsion angle between the donor and acceptor frame of ∼62°. Because of the low rotational barrier,


DOI: 10.1021/acs.jctc.5b00501
J. Chem. Theory Comput. 2015, 11, 4316−4327

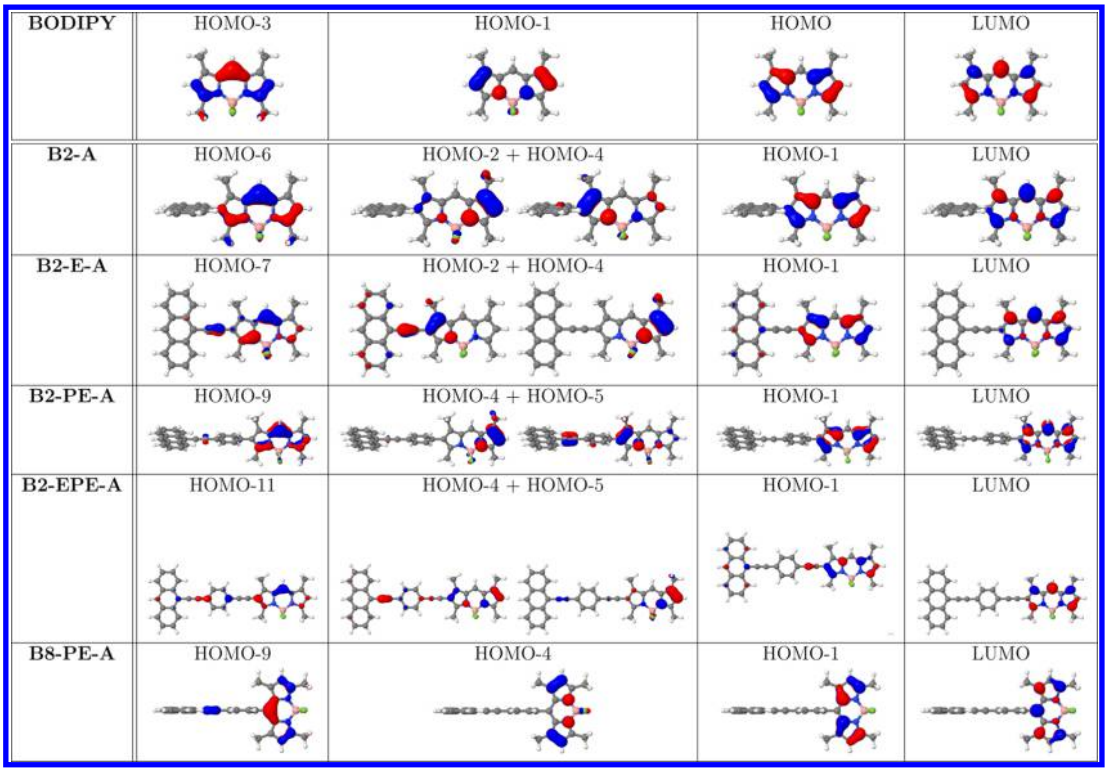


**Figure 8.** Frontier orbitals of BODIPY involved in the $S_0 \rightarrow S_1$ transition and their corresponding orbitals computed for the EET cassettes. For all EET cassettes except for **B8-PE-A**, HOMO−1 of BODIPY is recovered as a linear combination of two orbitals.

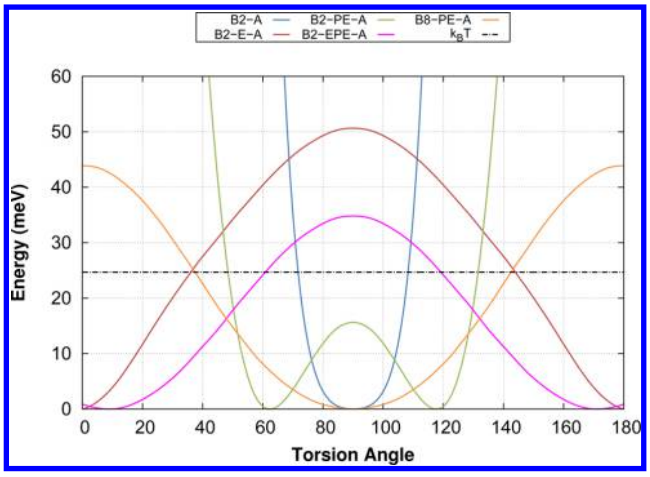


**Figure 9.** Unrelaxed electronic ground-state scans of the torsion angle between the planes of BODIPY and anthracene (B3LYP level of theory, steps of 1°). The linker was fixed perpendicular to the BODIPY frame in **B8-PE-A**. In **B2-PE-A** and **B2-EPE-A**, the linker was kept in plane with anthracene. All values are given with respect to the conformation that yields the lowest energy. Structures with an energy lower than $k_BT$ are assumed to be thermally occupied.

structures with dihedrals between 50° and 130° are assumed to be occupied. In **B8-PE-A**, a perpendicular orientation is preferred, because of the steric interaction between the methyl groups located at C1 and C7 of BODIPY and the adjacent phenyl ring of the linker. The torsion angle may change up to 55° around the global minimum. Nevertheless, the torsion angle does not significantly influence the EC coupling matrix element, since it does not change the relative orientation of the transition dipole moments. The dihedreal angles between the donor and the acceptor moieties in the relaxed ground-state geometries of the cassettes slightly deviate from those of the unrelaxed scans, particularly because of relaxation of the methyl groups and the phenyl rings.

**3.4. Excitonic Coupling.** In the framework of TSEET, the molecular linker is not directly involved in the EET but serves as a spacer conserving a certain distance and the relative orientation of the donor and the acceptor. This situation is described in our fragmentation model I. Our fragmentation model II takes also parts of TBEET into account while neglecting charge-transfer (CT) contributions. Excitonic couplings between BODIPY and anthracene calculated with the two different fragmentation models are shown in Table 2. Among the EET cassettes examined in this work, **B2-A** is the one with the smallest donor−acceptor distance. In this cassette, C2 of BODIPY is directly linked to C9 of anthracene. Using MTD and fragmentation model I, we find a value of 1141 $cm^{-1}$ for the direct contribution and a value of 30.0 $cm^{-1}$ for the exchange contribution. Because of the small intermolecular distance of only 6.3 Å, the direct contribution is very high and the exchange contribution is not negligibly small. A substantially smaller value of 983 $cm^{-1}$ for the direct contribution is obtained in the IDA. As already discussed for the ethylene dimer, IDA underestimates the exact EC at small distances, because of the limitations of the multipole expansion. With regard to the relative orientation of BODIPY and anthracene in this cassette, EC is maximal because the transition dipole moments are oriented in a parallel manner. In **B2-E-A**, **B2-PE-A**, and **B2-EPE-A**, the arrangement is essentially identical but the distance is successively increased. Concomitantly, direct contribution and exchange contributions successively become smaller. The exchange contribution decreases much faster than the direct contribution. It exhibits a value of 3.5 $cm^{-1}$ for **B2-E-A** and is found to be zero in the case of all other EET cassettes. For a donor−acceptor distance


DOI: 10.1021/acs.jctc.5b00501
J. Chem. Theory Comput. 2015, 11, 4316−4327

**Table 2. Direct and Exchange Contributions to the EC Matrix Elements, as Well as EET Rates of the Studied EET Cassettes Calculated with Different Models**

| | B2-A | B2-E-A | B2-PE-A | B2-EPE-A | B8-PE-A |
|---|---|---|---|---|---|
| **$S_0$ Geometry (Fragmentation Model I)** | | | | | |
| spectral overlap integral (cm) | | | $1.06 \times 10^{-5}$ | | |
| IDA | | | | | |
| $\lvert J_{DA}\rvert$ ($cm^{-1}$) | 983 | 350 | 109 | 63 | 0.0 |
| MTD | | | | | |
| $\lvert J_{DA}\rvert$ ($cm^{-1}$) | 1141 | 423 | 119 | 67 | 0.0 |
| $\lvert K_{DA}\rvert$ ($cm^{-1}$) | 30.0 | 3.5 | 0.0 | 0.0 | 0.0 |
| EET rate ($s^{-1}$) | $2.3 \times 10^{13}$ | $3.2 \times 10^{12}$ | $2.6 \times 10^{11}$ | $8.3 \times 10^{10}$ | $4.3 \times 10^{0}$ |
| **Acceptor $S_0$, Donor $S_1$ Geometry (Fragmentation Model I)** | | | | | |
| spectral overlap integral (cm) | | | $1.06 \times 10^{-5}$ | | |
| MTD | | | | | |
| $\lvert J_{DA}\rvert$ ($cm^{-1}$) | 1140 | 426 | 123 | 69 | 0.0 |
| $\lvert K_{DA}\rvert$ ($cm^{-1}$) | 30.0 | 3.1 | 0.0 | 0.0 | 0.0 |
| EET rate ($s^{-1}$) | $2.3 \times 10^{13}$ | $3.3 \times 10^{12}$ | $2.8 \times 10^{11}$ | $8.8 \times 10^{10}$ | $2.5 \times 10^{0}$ |
| **MD Snapshots (Fragmentation Model I)** | | | | | |
| spectral overlap integral (cm) | | | $1.06 \times 10^{-5}$ | | |
| MTD | | | | | |
| $\lvert J_{DA}\rvert$ ($cm^{-1}$) | 951 | 377 | 114 | 62 | 6.9 |
| EET rate ($s^{-1}$) | $2.1 \times 10^{13}$ | $2.8 \times 10^{12}$ | $2.7 \times 10^{11}$ | $7.1 \times 10^{10}$ | $1.62 \times 10^{9}$ |
| **$S_0$ Geometry (Fragmentation Model II, Spectral Overlap of Monomers)** | | | | | |
| spectral overlap integral (cm) | | | $1.06 \times 10^{-5}$ | | |
| MTD | | | | | |
| $\lvert J_{DA}\rvert$ ($cm^{-1}$) | | 1013 | 766 | 678 | 0.0 |
| $\lvert K_{DA}\rvert$ ($cm^{-1}$) | | 92 | 27 | 46 | 0.0 |
| EET rate ($s^{-1}$) | | $1.6 \times 10^{13}$ | $1.0 \times 10^{13}$ | $7.3 \times 10^{12}$ | $9.9 \times 10^{2}$ |
| **$S_0$ Geometry (Fragmentation Model II, Adapted Spectral Overlap)** | | | | | |
| spectral overlap integral (cm) | | $8.39 \times 10^{-5}$ | $2.46 \times 10^{-4}$ | $1.79 \times 10^{-4}$ | $2.46 \times 10^{-4}$ |
| MTD | | | | | |
| $\lvert J_{DA}\rvert$ ($cm^{-1}$) | | 1013 | 766 | 678 | 0.0 |
| $\lvert K_{DA}\rvert$ ($cm^{-1}$) | | 92 | 27 | 46 | 0.0 |
| EET rate ($s^{-1}$) | | $8.4 \times 10^{13}$ | $1.6 \times 10^{14}$ | $8.4 \times 10^{13}$ | $1.6 \times 10^{4}$ |
| **MD Snapshots (Fragmentation Model II, Adapted Spectral Overlap)** | | | | | |
| spectral overlap integral (cm) | | | | | $2.46 \times 10^{-4}$ |
| MTD | | | | | |
| $\lvert J_{DA}\rvert$ ($cm^{-1}$) | | | | | 18 |
| EET rate ($s^{-1}$) | | | | | $1.5 \times 10^{11}$ |
| exp. EET rate[19] ($s^{-1}$) | $>5.0 \times 10^{12}$ | $>5.0 \times 10^{12}$ | $>5.0 \times 10^{12}$ | $>5.0 \times 10^{12}$ | $2.5 \times 10^{12}$ |

of more than 15 Å (**B2-EPE-A**), IDA and MTD almost provide the same result. Therefore, we strongly recommend that MTD be used for EET cassettes with small molecular linkers.

On the basis of fragmentation model I, we further examined how the relaxation of the anthracene scaffold to its $S_1$ state geometry affects the size of the EC matrix elements (Table 2). For **B2-E-A**, we find an increase of the direct contribution by only 3 $cm^{-1}$ out of 423 $cm^{-1}$ in the MTD approach, corresponding to a change by 0.7%. The exchange contribution differs by 0.4 $cm^{-1}$. On a relative scale, the latter change is larger (i.e., 11.4%). Nevertheless, we consider these changes to be negligible. The direct EC matrix elements of the larger cassettes increase slightly. From these results, we conclude that a possible relaxation of the donor to its $S_1$ state geometry has only a minor effect the EC matrix element. This justifies the use of donor and acceptor geometries directly derived from the electronic ground state of the EET cassette without any further optimization.

Furthermore, we tested the influence of the atomic orbital basis set on the size of the EC, taking the example of **B2-E-A**. Within the IDA, the EC increases by only 0.6% if the large TZVP basis set is used instead of the SVP basis. The EC computed within the MTD approach is not affected much by an enhanced description of the EC in **B2-E-A** either. The direct contribution to EC decreases by 11 $cm^{-1}$, to a value of 421 $cm^{-1}$, if the TZVP basis set is used, while the exchange contribution increases by 0.4 $cm^{-1}$, to a value of 3.91 $cm^{-1}$.

Although the donor and acceptor moieties in BODIPY-based EET cassettes are connected covalently by a molecular bridge, there is no obvious way for TBEET.[16] To get an estimate how strongly the linker affects the EC, we applied fragmentation model II. The MOs of the cassettes are largely localized on the donor and the acceptor parts of the system, respectively, and correspond quite well to the frontier orbitals computed for the monomers (see Figures 6 and 8). This holds true best for **B2-A**, since the donor and the acceptor are directly linked in a perpendicular orientation. In all other EET cassettes, we find a slight extension of some of the involved MOs to the linker moiety, indicating an additional contribution of the linker to the EC. Among the frontier orbitals, the HOMO of the donor and the LUMO of the acceptor may be assumed to be the two most important orbitals involved in the EC. As may be seen in


DOI: 10.1021/acs.jctc.5b00501
J. Chem. Theory Comput. 2015, 11, 4316−4327

Figure 6, the electron density contribution of the HOMO of all investigated cassettes is mainly located on the donor but extends markedly to the linker atoms. In contrast, no linker contributions are observed for the LUMO (Figure 6), which appears to be an almost-pure acceptor MO. Hence, the molecular linker was assigned to the donor fragment. Using fragmentation model II, we find higher direct contributions of the EC, which decrease much more slowly as the size of the linker increases (see Table 2). The exchange contributions are still very small, compared to the direct contributions, but now are clearly different from zero. In **B8-PE-A**, the direct and exchange contributions are found to be extremely small in the minimum nuclear arrangement with both fragmentation models, because the transition dipole moments of BODIPY and anthracene are oriented in an almost-perpendicular manner. The influence of the EC on the EET rate will be discussed in the next section.

**3.5. EET Rates.** EET rates were calculated from the spectral overlap and the EC obtained with the MTD approach (Table 2). Since the spectral overlap of $1.06 \times 10^5$ cm is constant for a given donor−acceptor pair in fragmentation model I, the highest EET rate is observed for the EET cassette with the shortest linker. For **B2-A**, in which donor and acceptor are separated only by a single C−C bond, we obtain an EET rate of $2.3 \times 10^{13}$ $s^{-1}$. Fragmentation models I and II do not differ for this cassette. Since the exchange contribution to the EC is extremely small, compared to the direct contribution, it has only a very slight influence on the total EET rate. For all other cassettes, in which the transition dipole moments of anthracene and BODIPY are oriented in a parallel manner, the calculated EET rates are smaller, ranging from $3.2 \times 10^{12}$ $s^{-1}$ to $8.3 \times 10^{10}$ $s^{-1}$, depending on the length of the molecular linker. Kim et al.[19] found EET rates higher than the temporal resolution of their experiment ($5.0 \times 10^{12}$ $s^{-1}$) for all cassettes with a parallel orientation of the transition dipole moments. While **B2-A** and **B2-E-A** perfectly agree with the experimental evidence, the calculated EET rates of **B2-PE-A** and **B2-EPE-A** are smaller by 1 and 2 orders of magnitude, respectively, indicating an increasing influence of the linker. In **B8-PE-A**, in which the transition dipole moments of the donor and the acceptor are oriented in an almost-perpendicular manner, the calculated EET rate is extremely small ($4.3 \times 10^0$ $s^{-1}$). Concomitantly, the calculated EET rate is significantly smaller than the experimental value of $2.5 \times 10^{12}$ $s^{-1}$.

For that reason, we investigated the influence of dynamic effects with the help of short *ab initio* MD simulations. We found that the angle between the transition dipole moments of BODIPY and anthracene changes due to vibration. In **B8-PE-A**, the average displacement from the dihedral between the donor and acceptor moieties of the relaxed ground-state structure amounts to ∼5° (Figure 10). Since the EC matrix element is minimal at 90°, sampling of the vibrational motion leads to an increased direct contribution and, hence, to an increased average EET rate ($1.62 \times 10^9$ $s^{-1}$). Unfortunately, this rate is still smaller than the experimental value by ∼3 orders of magnitude. In the other EET cassettes, vibrational averaging decreases the direct contribution to the EC between BODIPY and anthracene. Nevertheless, the effect is much weaker and the mean EET rates are only slightly smaller than those calculated for the static case. This behavior can be explained by considering the angular dependency of the EC. When the transition dipole moments of the donor and the acceptor are oriented in a parallel manner, the EC is large. At this point, the slope which describes the change of the EC with the torsion angle is minimal. Thus, a small change of the torsion angle due to molecular vibrations causes only a small decrease of the EC. When the transition dipole moments are oriented in a perpendicular manner, as in the case of **B8-E-A**, the EC is zero but the slope is maximal. Thus, only small changes of the torsion angle cause a large change of the EC. Independent of the relative orientation of the transition dipole moments, the longer the molecular linker, the more significant the dynamic effects.

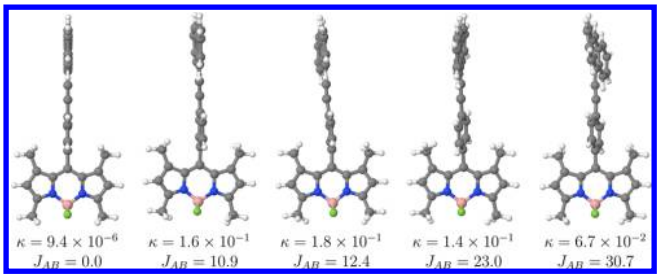


**Figure 10.** Selected snapshots of the MD simulation of **B8-PE-A**. $J_{AB}$ denotes the direct coupling of the appropriate snapshot (given in units of $cm^{-1}$). Orientation factor $\kappa$ indicates the relative orientation of the transition dipole moments.

The influence of the structure of the molecular linker is estimated by fragmentation model II. Assuming an unchanged spectral overlap integral, we find EET rates ranging from $1.6 \times 10^{13}$ $s^{-1}$ (**B2-E-A**) to $7.3 \times 10^{12}$ $s^{-1}$ (**B2-EPE-A**) for all EET cassettes in which the transition dipole moments are oriented in a parallel manner. For **B8-PE-A**, we calculated an EET rate of $1.0 \times 10^3$ $s^{-1}$, which is still far from the experimentally predicted value. All calculated rates are higher by 1 to 2 orders of magnitude, compared to the results obtained with fragmentation model I but subsequently decrease with increasing length of the linker as well. Analyzing the $S_0 \rightarrow S_1$ transitions of the donor fragments, we find a decrease of the vertical excitation energy and an increase of the transition dipole moment with increasing size of the linker, when compared to the plain donor. The influence on the spectral overlap integral is crudely estimated by a red-shift of the emission spectrum of anthracene by the appropriate energy difference. Since the shifted donor emission spectrum and the unshifted acceptor absorption spectrum come closer, we find an increasing spectral overlap integral with increasing length of the linker. Taking both altered EC and spectral overlap integral into account, we find the highest EET rate of $1.6 \times 10^{14}$ $s^{-1}$ for **B2-PE-A**. For **B2-E-A** and **B2-EPE-A**, we find very similar rates ($8.4 \times 10^{13}$ $s^{-1}$), which are in the range of the rate of **B2-A**, in which the donor and acceptor are directly linked via a single C−C bond. All calculated rates are in perfect agreement with experimental findings, predicting EET rates that are higher than the experimental lower limit of $5.0 \times 10^{12}$ $s^{-1}$.[19] Not unexpectedly, the rate calculated for **B8-PE-A**, using a static model ($1.6 \times 10^4$ $s^{-1}$), is much smaller than the experimental value. Considering dynamic effects, the EET rate becomes $1.5 \times 10^{11}$ $s^{-1}$, which is too small by only 1 order of magnitude.

## 4. CONCLUSIONS

The EET rate in five different BODIPY-based EET cassettes has been determined with quantum chemical methods. To this end, a computer program was devised that calculates the through-space contributions to the EET rates either in the IDA


DOI: 10.1021/acs.jctc.5b00501
J. Chem. Theory Comput. 2015, 11, 4316−4327

or from monomer transition densities of DFT/MRCI wave functions. The correctness of the program was validated by benchmark calculations on a small homodimeric model system of two $\pi$-stacked ethylene molecules. Not unexpectedly, the IDA fails to describe the EC at small intermolecular distances. In contrast, the DFT/MRCI-based MTD is found to be a powerful method to approximate the EC and EET rates in EET cassettes with dominant through-space contributions.

Experimental absorption and emission spectra of the acceptor and donor units of the EET cassettes, BODIPY and anthracene, respectively, are reproduced well by vibrationally resolved computed spectra. In the cassettes with short to medium-long molecular linkers, we find that IDA produces significantly smaller EC matrix elements than MTD. Therefore, MTD was chosen for the calculation of the EET rates. For all EET cassettes in which the transition dipole moments of donor and acceptor are oriented in a parallel manner, we find EET rates in the order of the temporal resolution of the experiment[19] when fragmentation model II is used, i.e., when contributions from the molecular linker are taken into account in an approximate manner. If the simpler fragmentation model I is applied to EET cassettes with a longer linker, the EET rates become significantly too small. For **B8-PE-A**, in which the transition dipole moments are oriented in a perpendicular manner, dynamic effects play an important role, increasing the computational EET rate by up to 10 orders of magnitude, compared to the static model.

One reason for the deviations of the calculated EET rate of **B8-PE-A** from the experimental values[19] may be that charge-transfer (CT) contributions are not considered in our calculations. In $\pi$-stacked electronically excited perylene-bisimide aggregates, such contributions have been shown to be important.[55] Furthermore, our consideration of the influence of the nuclear motion is only based on very short MD trajectories. More exact rates may be obtained either from longer force-field-based MD simulations or by including vibronic interactions through a Taylor expansion about the Franck–Condon point. Work along these lines is in progress.

## AUTHOR INFORMATION


### Corresponding Author

*Tel.: +49 211 81-13210. Fax: +49 211 81-13466. E-mail: Christel.Marian@uni-duesseldorf.de.


### Notes

The authors declare no competing financial interest.

## ACKNOWLEDGMENTS

Financial support by the Deutsche Forschungsgemeinschaft (through No. TA 725/1-1) is gratefully acknowledged.

## REFERENCES


(1) Förster, T. *Ann. Phys. (Berlin, Ger.)* **1948**, *437*, 55–75.
(2) Dexter, D. L. *J. Chem. Phys.* **1953**, *21*, 836–850.
(3) McConnell, H. M. *J. Chem. Phys.* **1961**, *35*, 508–515.
(4) Pourtois, G.; Beljonne, D.; Cornil, J.; Ratner, M. A.; Brédas, J. L. *J. Am. Chem. Soc.* **2002**, *124*, 4436–4447.
(5) May, V.; Kühn, O. *Charge and Energy Transfer Dynamics in Molecular Systems*; Wiley–VCH: Weinheim, Germany, 2004.
(6) Hennebicq, E.; Pourtois, G.; Scholes, G. D.; Herz, L. M.; Russell, D. M.; Silva, C.; Setayesh, S.; Grimsdale, A. C.; Müllen, K.; Brédas, J.-L.; et al. *J. Am. Chem. Soc.* **2005**, *127*, 4744–4762.
(7) Fückel, B.; Köhn, A.; Harding, M. E.; Diezemann, G.; Hinze, G.; Basché, T.; Gauss, J. *J. Chem. Phys.* **2008**, *128*, 074505.
(8) Stehr, V.; Engels, B.; Deibel, C.; Fink, R. *J. Chem. Phys.* **2014**, *140*, 024503.
(9) Dirac, P. A. M. *Proc. R. Soc. London, Ser. A* **1927**, *114*, 243–265.
(10) Fermi, E. *Nuclear Physics: A Course Given by Enrico Fermi at the University of Chicago*; University of Chicago Press: Chicago, IL, 1950 (ISBN: 9780226243658).
(11) Rousseau, T.; Cravino, A.; Bura, T.; Ulrich, G.; Ziessel, R.; Roncali, J. *Chem. Commun.* **2009**, 1673–1675.
(12) Rousseau, T.; Cravino, A.; Ripaud, E.; Leriche, P.; Rihn, S.; de Nicola, A.; Ziessel, R.; Roncali, J. *Chem. Commun.* **2010**, *46*, 5082–5084.
(13) Mueller, T.; Gresser, R.; Leo, K.; Riede, M. *Sol. Energy Mater. Sol. Cells* **2012**, *99*, 176–181.
(14) Chen, J. J.; Conron, S. M.; Erwin, P.; Dimitriou, M.; McAlahney, K.; Thompson, M. E. *ACS Appl. Mater. Interfaces* **2015**, *7*, 662–669.
(15) Bura, T.; Leclerc, N.; Fall, S.; Lévêque, P.; Heiser, T.; Retailleau, P.; Rihn, S.; Mirloup, A.; Ziessel, R. *J. Am. Chem. Soc.* **2012**, *134*, 17404–17407.
(16) Loudet, A.; Burgess, K. *Chem. Rev.* **2007**, *107*, 4891–4932.
(17) Briggs, E. A.; Besley, N. A.; Robinson, D. *J. Phys. Chem. A* **2013**, *117*, 2644–2650.
(18) Wan, C.-W.; Burghart, A.; Chen, J.; Bergström, F.; Johansson, L. B.-Å.; Wolford, M. F.; Kim, T. G.; Topp, M. R.; Hochstrasser, R. M.; Burgess, K. *Chem.—Eur. J.* **2003**, *9*, 4430–4441.
(19) Kim, T. G.; Castro, J. C.; Loudet, A.; Jiao, J. G.-S.; Hochstrasser, R. M.; Burgess, K.; Topp, M. R. J. *J. Phys. Chem. A* **2006**, *110*, 20–27.
(20) Caprasecca, S.; Curutchet, C.; Mennucci, B. *Photochem. Photobiol. Sci.* **2011**, *10*, 1602–1609.
(21) Hsu, C.-P. *Acc. Chem. Res.* **2009**, *42*, 509–518.
(22) Hsu, C.-P.; You, Z.-Q.; Chen, H.-C. *J. Phys. Chem. C* **2008**, *112*, 1204–1212.
(23) Blancafort, L.; Voityuk, A. A. *J. Chem. Phys.* **2014**, *140*, 095102.
(24) Fink, R.; Pfister, J.; Schneider, A.; Zhao, H.; Engels, B. *Chem. Phys.* **2008**, *343*, 353–361.
(25) Fink, R. F.; Pfister, J.; Zhao, H. M.; Engels, B. *Chem. Phys.* **2008**, *346*, 275–285.
(26) Fujimoto, K. J. *J. Chem. Phys.* **2012**, *137*, 034101.
(27) Wong, C. Y.; Curutchet, C.; Tretiak, S.; Scholes, G. D. *J. Chem. Phys.* **2009**, *130*, 081104.
(28) Davydov, A. S. *Sov. Phys. Usp.* **1964**, *7*, 145–178.
(29) Kasha, M.; Rawls, H. R.; Ashraf El-Bayoumi, M. *Pure Appl. Chem.* **1965**, *11*, 371–392.
(30) McWeeny, R. *Methods of Molecular Quantum Mechanics*; Academic Press: London, 1989; p 129.
(31) Stephens, P. J.; Devlin, F. J.; Chabalowski, C. F.; Frisch, M. J. *J. Phys. Chem.* **1994**, *98*, 11623–11627.
(32) *TURBOMOLE V6.5*, 2013. A development of University of Karlsruhe and Forschungszentrum Karlsruhe GmbH (1989–2007), TURBOMOLE GmbH, since 2007; available via the Internet at: http://www.turbomole.com.
(33) Schäfer, A.; Horn, H.; Ahlrichs, R. *J. Chem. Phys.* **1992**, *97*, 2571–2577.
(34) Neugebauer, J.; Reiher, M.; Kind, C.; Hess, B. A. *J. Comput. Chem.* **2002**, *23*, 895–910.
(35) Grimme, S.; Waletzke, M. *J. Chem. Phys.* **1999**, *111*, 5645–5655.
(36) Becke, A. D. *J. Chem. Phys.* **1993**, *98*, 1372–1377.
(37) Vahtras, O.; Almlöf, J.; Feyereisen, M. *Chem. Phys. Lett.* **1993**, *213*, 514–518.
(38) Weigend, F.; Häser, M.; Patzelt, H.; Ahlrichs, R. *Chem. Phys. Lett.* **1998**, *294*, 143–152.
(39) Caprasecca, S.; Mennucci, B. *J. Phys. Chem. A* **2014**, *118*, 6484–6491.
(40) Etinski, M.; Tatchen, J.; Marian, C. M. *J. Chem. Phys.* **2011**, *134*, 154105.
(41) Etinski, M.; Tatchen, J.; Marian, C. M. *Phys. Chem. Chem. Phys.* **2014**, *16*, 4740–4751.
(42) Allen, M. P.; Tildesley, D. J. *Computer Simulation of Liquids*; Clarendon Press: Oxford, U.K., 1987.



DOI: 10.1021/acs.jctc.5b00501
J. Chem. Theory Comput. 2015, 11, 4316–4327

(43) Godbout, N.; Salahub, D. R.; Andzelm, J.; Wimmer, E. *Can. J. Chem.* **1992**, *70*, 560−571.
(44) Platt, J. R.; Klevens, H. B.; Price, W. C. *J. Chem. Phys.* **1949**, *17*, 466−469.
(45) Levine, B. G.; Ko, C.; Quenneville, J.; Martínez, T. J. *Mol. Phys.* **2006**, *104*, 1039−1051.
(46) Filatov, M. *J. Chem. Theory Comput.* **2013**, *9*, 4526−4541.
(47) König, C.; Schlüter, N.; Neugebauer, J. *J. Chem. Phys.* **2013**, *138*, 034104.
(48) Marian, C. M.; Gilka, N. *J. Chem. Theory Comput.* **2008**, *4*, 1501−1515.
(49) Biermann, D.; Schmidt, W. *J. Am. Chem. Soc.* **1980**, *102*, 3163−3173.
(50) Parac, M.; Grimme, S. *Chem. Phys.* **2003**, *292*, 11−21.
(51) Ferguson, J.; Reeves, L. W.; Schneider, W. G. *Can. J. Chem.* **1957**, *35*, 1117−1136.
(52) Berlman, I. *Handbook of Fluorescence Spectra of Aromatic Molecules*; Academic Press: New York, 1971.
(53) Dixon, J. M.; Taniguchi, M.; Lindsey, J. S. *Photochem. Photobiol.* **2005**, *81*, 212−213.
(54) de Wael, E. V.; Pardoen, J. A.; van Koeveringe, J. A.; Lugtenburg, J. *Recl. Trav. Chim. Pays-Bas* **1977**, *96*, 306−309.
(55) Liu, W.; Settels, V.; Harbach, P. H.; Dreuw, A.; Fink, R. F.; Engels, B. J. *J. Comput. Chem.* **2011**, *32*, 1971−1981.


DOI: 10.1021/acs.jctc.5b00501
*J. Chem. Theory Comput.* 2015, 11, 4316−4327